Experimental studies of supercavitating flow about simple two-dimensional bodies in a jet

By EDWARD SILBERMAN
St Anthony Falls Hydraulic Laboratory, University of Minnesota

(Received 8 August 1958)

A two-dimensional free-jet water tunnel developed at the St Anthony Falls Hydraulic Laboratory of the University of Minnesota is described briefly. Results of experimental measurements on a two-dimensional cup, symmetrical wedges, inclined flat plates, and a circular cylinder in the tunnel are given.

Measured force coefficients at zero cavitation number are in good agreement with theory. Shapes of the cavities were computed for one of the wedges and for one of the plates at zero cavitation number; the observed shapes are also in good agreement with the theory.

For non-zero cavitation numbers, theoretical results for force coefficients were available for comparison in only two cases. For one of these, the cup, agreement between theory and experiment was good up to a cavitation number of about 0·5. For the other, a symmetrical wedge, experimental results were compared with a linear theory with good agreement for cavitation numbers between about 0·1 and 0·3. In the case of the wedge, measured cavity lengths were somewhat shorter than predicted by the linear theory. All other comparisons with theory at non-zero cavitation number had to be made with the theory as developed for infinite fluid. The experimental force coefficients were less than predicted by infinite-fluid theory, but tended to approach the theoretical values as the cavitation number increased. A similar tendency marked the comparison between the experimental data and data taken by others in closed tunnels.

1. Introduction

In modern technology, it has become desirable to operate hydrofoils at such speeds that steady-state (or quasi-steady-state) cavities are formed of lengths equal to or many times greater than the chord length of the foil. Conventional water tunnels are limited in their usefulness for studying such supercavitating flows by blockage at small cavitation numbers (cavitation number is defined by equation (1) below). The blockage problem has been fully discussed by Birkhoff, Plesset & Simmons (1950). There is no blockage problem in a free jet, however, and experimental studies of supercavitating flows can be conducted at extremely small cavitation numbers—even zero—in a suitably designed free-jet tunnel.

A brief description of a two-dimensional, free-jet water tunnel developed at the St Anthony Falls Hydraulic Laboratory of the University of Minnesota is contained herein, together with the results of some experimental measurements on

simple, two-dimensional bodies (the cup, symmetrical wedge, inclined flat plate, and circular cylinder). The experimental results are compared with theoretical predictions and with measurements by others in closed tunnels, when available.

The usefulness of experimental measurements of supercavitating flows obtained in a water tunnel is limited by the problem of converting data from tunnel boundary conditions to infinite fluid. Some discussion of this problem for a free-jet tunnel has appeared in the literature (e.g. Birkhoff, Plesset & Simmons (1952) and Cohen & Tu (1956)); and it is known that, in general, cavity lengths will be shorter and drag coefficients will be less in a free jet than in infinite fluid. A better quantitative idea of these wall corrections than previously available may be obtained by comparing the present experimental results and related theory with the theory for infinite fluid and experimental results for closed tunnels. In fact, the purpose of the experimental programme described herein was to investigate the utility of the two-dimensional free-jet tunnel for studying supercavitating flows in infinite fluid.

2. The free-jet tunnel

Figure 1 illustrates the free-jet tunnel and figure 2 (plate 1) shows the two-dimensional test section. The entire test section is enclosed by a sealed housing when the tunnel is in operation. The housing creates an evacuated chamber through which the jet passes. The tunnel was originally designed as an axially symmetric jet of 10 in. diameter. A detailed description of the basic tunnel was given by Christopherson (1953). The tunnel is not recirculating but draws water directly from a river supply and wastes it to the river at a lower level.

As may be seen in figure 1, the axis of the jet is vertical, and the test section has been placed at such a height that the region surrounding the jet at the test section may be maintained at vapour pressure by the weight of the suspended water column in the vertical conduit. Pressures intermediate between vapour pressure and atmospheric pressure may be obtained by admitting atmospheric air to the test section, thereby lowering the water column. The maximum velocity available in the tunnel is 50 ft./sec, but this maximum is reduced as the operating pressure is increased by admitting air.

The tunnel is made two-dimensional by inserting two parallel, flat plates into the jet as shown in figure 2 (plate 1). Each plate is $\frac{3}{8}$ in. thick by 7 in. wide and the plates are 5 in. apart, fixing the span of test bodies at 5 in. The jet varies in width between the 10 in. width of the original axially symmetric tunnel at the plane of symmetry and about 8·7 in. at the side plates. (The side plates are completely surrounded by the jet; only the support structure penetrates the jet walls.) The nominal width of the jet is taken as 10 in.

The plates extend 3·5 ft. downstream from the test-body location; this length brings the ends of the plates to the top of the water column when the tunnel is operated at minimum pressure. When the cavity length produced by a given test body exceeds about 3·5 ft. or when the cavity width exceeds about 7 in., the cavity breaks out or vents to the surrounding chamber, splitting the cavity and producing a cavitation number which is effectively zero. There is, therefore, a gap

in the cavitation numbers obtainable in the tunnel between zero and the cavitation number corresponding to a 3·5 ft. long or 7 in. wide cavity. The plates extend about 6 in. upstream from the test body, and their leading edges are shaped so as to produce minimum cavitation. (The final shape was determined by trial and error in the tunnel.)

Each plate is made from a single sheet of brass, but one of the plates contains a plane Plexiglas window fitted smoothly into the brass. The upper edge of the

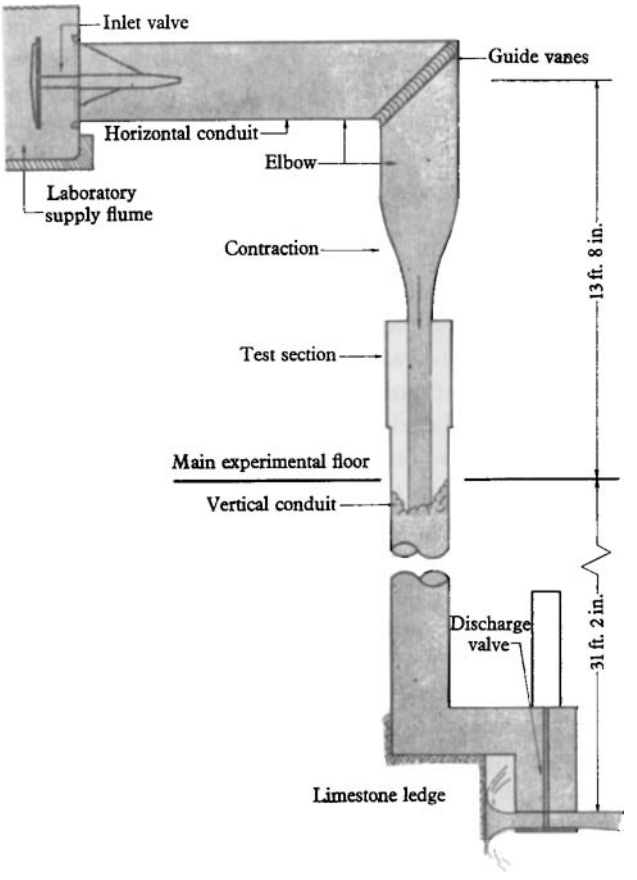

FIGURE 1. General scheme of water tunnel.

window is about 1·5 in. downstream from the centre of the test-body location. In line with this window, there is another window in the chamber housing; this second window is curved on the inside so as to come just into contact with the 10 in. axially symmetric jet, and is flat on the outside. Profiles of two-dimensional cavities may be inspected and photographed through these windows. One difficulty inherent in the window arrangement is that frequently the water between the two windows cavitates before the minimum cavitation number for the test body is reached, thus precluding observation at the lowest cavitation numbers. (It has been determined by photographing a grid in the tunnel that distortion through the windows is negligible.)

The brass wall opposite the window wall is provided with two pressure taps located about 1·5 in. downstream from the centre of the test-body location. One or both of these can be used to measure cavity pressure or to admit air to a cavity.

Each side plate houses a removable dynamometer, drag being measured on one side and lift on the other. (Because the jet is symmetrical, it is assumed that half the drag and half the lift are supported on each side.) Strain gauges are used as the sensing elements in the dynamometers. Each dynamometer is wafer-like, being $\frac{3}{16}$ in. thick and of $2\frac{1}{2}$ in. diameter, and is fitted into a 2·56 in. diameter recess in the corresponding side plate. As used in the experiments to be described, the drag dynamometer measures up to 20 lb., and the lift dynamometer up to 80 lb. within the linear calibration range. The dynamometer readings are repeatable in static calibration within about 1 % of full scale; in use, however, fluctuation of the load makes it necessary to read average forces, and accuracy to 1 % cannot be claimed. Interactions between lift, drag, and moment are very small and are eliminated by dead-weight calibration. The moment is not measured.

Each dynamometer recess is covered on the test-body side by disks 2·54 in. in diameter which are an integral part of the test body. Bodies and disks are made from stainless steel and oven-brazed to each other. The disks are 5·00 in. apart and, when in place, form a smooth continuation of the two-dimensional plates with a 0·01 in. annular gap. Load is transferred from a test body to the dynamometers through circular hubs on the disks which fit snugly into holes in the dynamometer. Set screws keep the hubs from turning or moving endwise, once angle of attack has been established. Application of load produces a small displacement in part of the dynamometer and in the covering disks. The annular gap thus becomes asymmetrical. There is some leakage through the annular gap, and this leakage sometimes interferes with cavity observation; but the leakage does not appear to influence force measurements.

Water velocity is determined by measuring the pressure drop in the nozzle leading to the jet. The pressure drop was previously calibrated against velocity by weighing the discharge up to velocities of about 30 ft./sec; the calibration curve was linear up to this velocity, and the straight line was extended to the highest velocities. The calibration curve was verified by measurements in the jet with a Pitot-static tube up to the highest velocities. These measurements also demonstrated that the velocity between the side plates at the test-body location, at 40 ft./sec. mean velocity, was uniform within 1 %; any boundary layer was confined to a region $\frac{1}{4}$ in. thick near each wall which could not be reached by the Pitot-static tube. This uniform velocity profile makes it possible, for computational purposes, to consider the flow to be that of an ideal, infinite, two-dimensional jet rather than a jet from a nozzle.

The calibrated velocity occurs at the end of the nozzle. The actual velocity head at the test body is composed of the velocity head at the nozzle exit plus the vertical distance from nozzle exit to centre of test body—7 in. in this tunnel. That this is the case was verified by measurements with a total-head tube with no body in the tunnel.

3. Experimental results

Some observed force coefficients are shown in figures 3 to 6. Cavity lengths, measured from photographs, are given in figure 7. Typical photographs are shown in figure 8 (plate 2). The shapes investigated were a two-dimensional cup (figure 3), two symmetrical wedges (figure 4), flat plates at four angles of attack (figure 5), and a circular cylinder (figure 6).

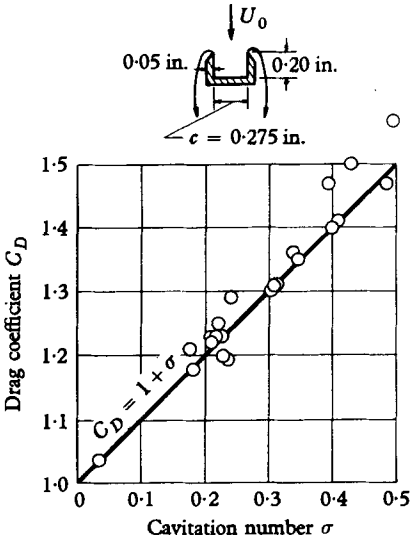

FIGURE 3. Drag coefficient for two-dimensional cup.

In presenting the data, the following parameters are used:

cavitation number $$\sigma = (p_0 - p_k)/q, \tag{1}$$

or $$\sigma_v = (p_0 - p_v)/q, \tag{1a}$$

lift coefficient $$C_L = L/lcq, \tag{2}$$

drag coefficient $$C_D = D/lcq, \tag{3}$$

Reynolds number $$\mathrm{Re} = U_0 c/\nu. \tag{4}$$

Here p_0 is the measured pressure in the chamber surrounding the jet, p_k is the measured cavity pressure, p_v is the vapour pressure of water at the operating temperature, $q = \frac{1}{2}\rho U_0^2$ is the reference dynamic pressure, U_0 is the velocity which would exist in the undisturbed jet at the position of the centre of the test body, L is the lift or net force on the body normal to U_0, D is the drag or net force on the body parallel to U_0, c is the chord length or other characteristic dimension of the body, l is the span (5 in. in this tunnel), ρ is the density of the water, and ν is the coefficient of kinematic viscosity of the water.

In the case of one of the wedges (figure 4*b*) and for the circular cylinder (figures 6*b* and 6*c*), the experiments were carried into the non-cavitating range. In these two cases the cavitation number is defined by (1*a*) because it was impossible to measure cavity pressure directly. All other experiments were limited

to the very small cavitation numbers associated with supercavitating flows; cavity pressure was measured directly and cavitation number is defined by (1). Almost all the data were obtained in a range of velocities U_0 from about 38 to 45 ft./sec. Some data were obtained at velocities as low as 20 ft./sec; these data are appropriately indicated where they occur.

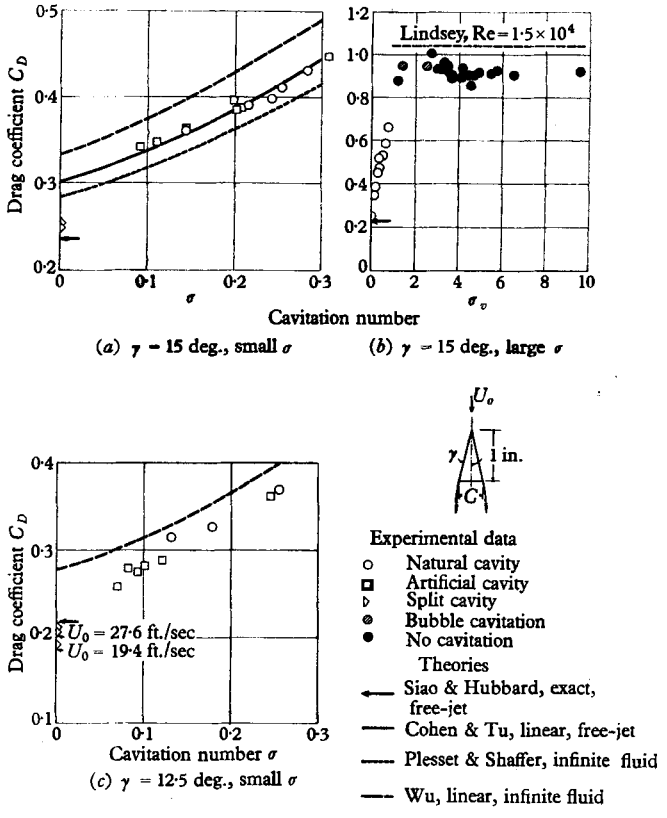

FIGURE 4. Drag coefficients for symmetrical wedges.

The lift L was taken directly from measured data for use in (2). The drag coefficient according to (3) was corrected, before plotting the data, by subtracting the calculated skin-friction drag coefficient for the end disks and the calculated skin-friction coefficient for the test body. The corrections are described in Appendix A. Therefore, the plotted drag coefficients relate to form or cavitation drag of the test bodies.

For the flat plates at small angles of attack, it was found that the drag coefficient, especially, was very sensitive to the sharpness of the leading edge. These edges were kept honed, and the tunnel was stopped and the edges were cleaned after each measurement was obtained. (Bits of grass from the river water accumulated on the leading edges.) Nevertheless, the drag data were difficult to reproduce, as may be seen in figures 5*a* and 5*c*.

Three different classes of cavities were generated. Naturally occurring, closed cavities are indicated by circles in the force-coefficient graphs. These cavities are

produced by controlling the parameters p_0 and q in equation (1). Closed cavities obtained by extending control to p_k by feeding air to the wakes of the bodies are indicated by square symbols and are called 'artificial'. Split cavities, illustrated

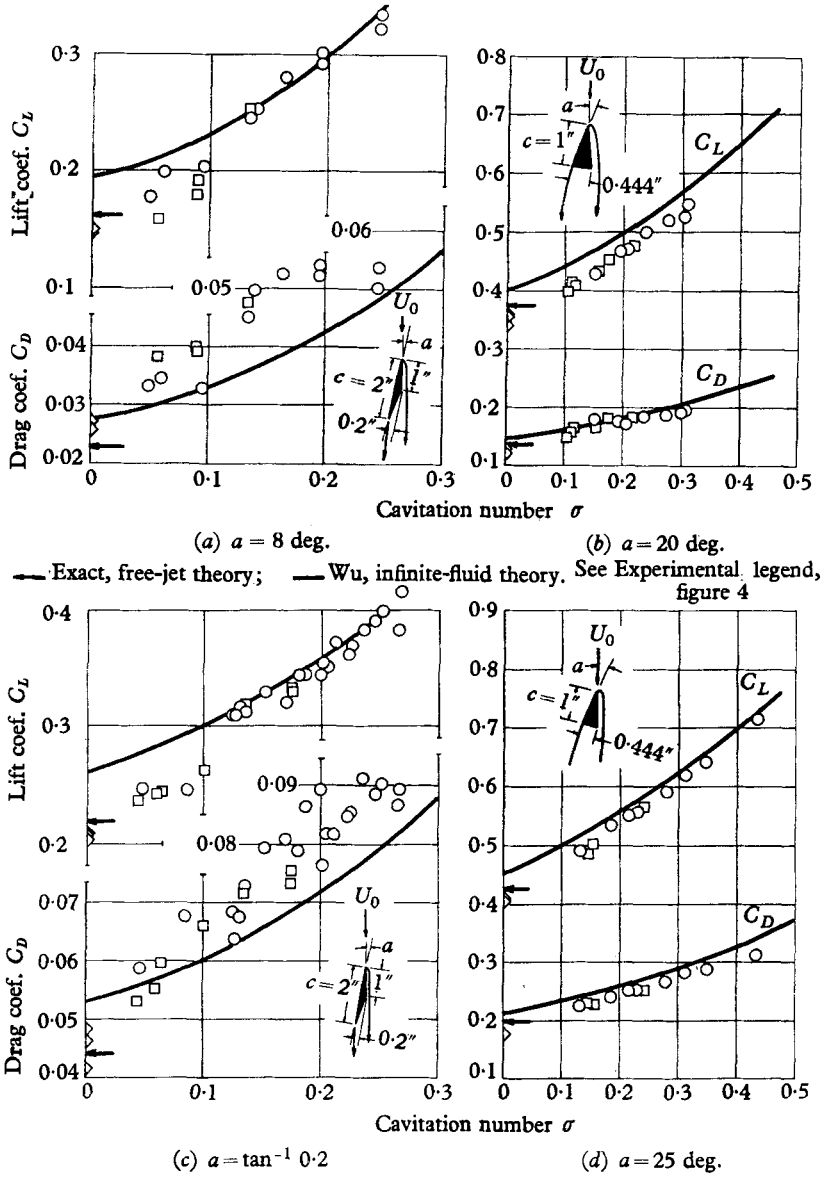

FIGURE 5. Lift and drag coefficients for inclined flat plates.

by photographs in figures 8*a* and 8*b* (plate 2), occur when a cavity is vented to the surrounding chamber; they are indicated by half-diamond-shaped symbols. There is an advantage in operating with an artificial cavity because, for the same cavitation number, q can be smaller and p_0 larger than for a natural cavity. With small q and large p_0, secondary cavitation of the leading edges of the side plates and of the space between the observation windows can be reduced or eliminated.

The experimental data indicate that there is no significant difference between natural and artificial cavities.

Visual observation showed that the cavity walls were generally laminar as they left the test bodies, except in the case of the 2 in. chord flat plates. The laminar

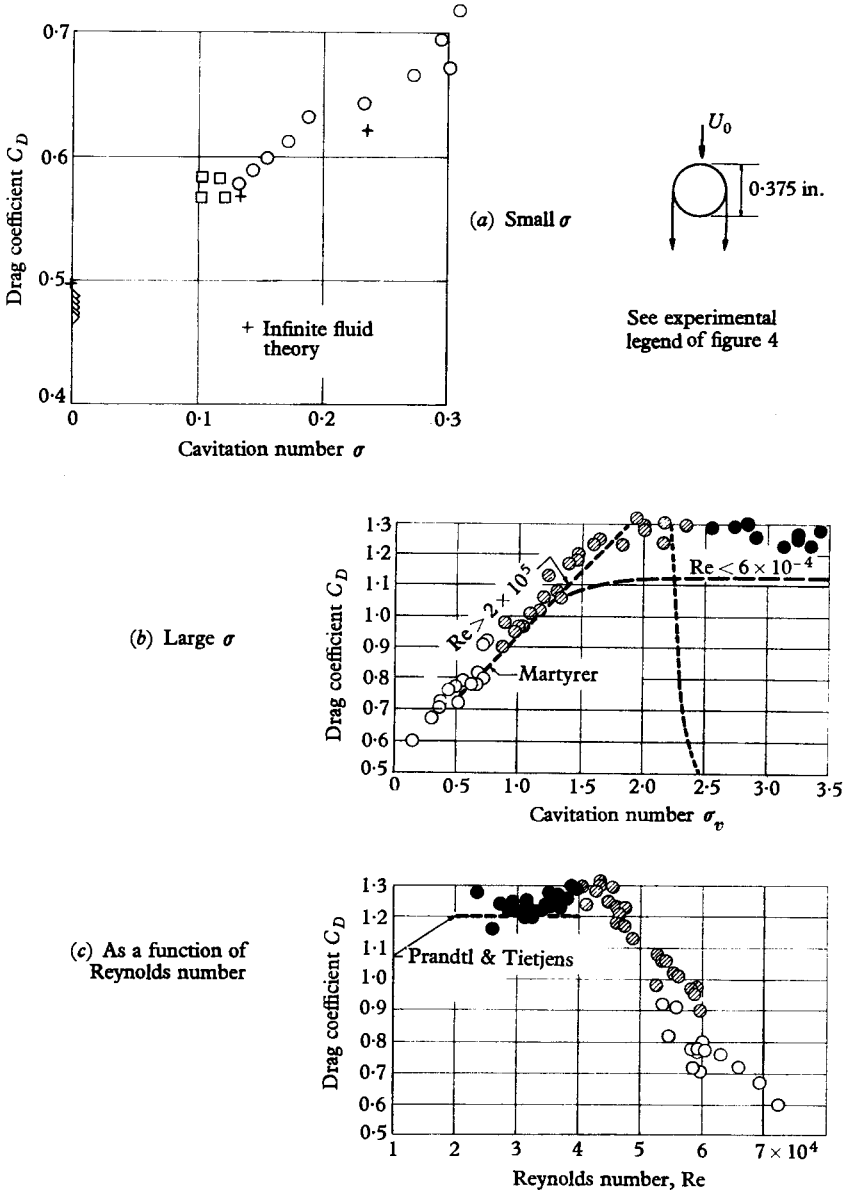

FIGURE 6. Drag coefficient for circular cylinder.

flow became turbulent within about 1 chord length or less from the trailing ends of the bodies. Transition appeared to occur along a fixed ragged line across the span on each cavity wall.

4. Effect of gravity

It is desirable to compare the experimental results with theoretical computations. As has already been mentioned in describing the equipment, the uniformity of the velocity across the jet makes it possible to treat the flow as that of an ideal, two-dimensional, infinite jet. A possible limitation on this treatment is the effect

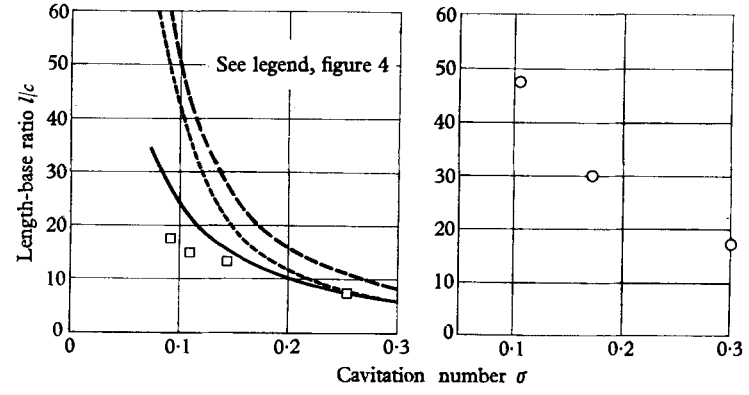

FIGURE 7. Typical cavity length measurements.

of gravity, because the jet is vertical and contracts as it falls. (The contraction effect attributable to gravity is, however, at least partially balanced by boundary-layer growth on the two-dimensional side plates.)

The magnitude of the gravitational effect depends on the Froude number of the jet. This is apparent from the continuity equation, which may be written

$$\frac{db}{dh} = -\frac{b}{U}\frac{dU}{dh}, \tag{5}$$

and from the momentum equation

$$U\frac{dU}{dh} = g, \tag{6}$$

where h is the depth from the origin of the jet to any point in the test section, U is the velocity at depth h, b is the breadth of the jet at depth h, and g is the acceleration due to gravity. Thus, we have

$$\frac{db}{dh} = -\frac{bg}{U^2}, \tag{7}$$

where the quantity on the right-hand side is the inverse square of the Froude number. For the test jet, b is 10 in.; with $U = 40$ ft./sec, the theoretical rate of contraction is approximately 0·2 in./ft. of fall, while at 20 ft./sec it is 0·8 in./ft.

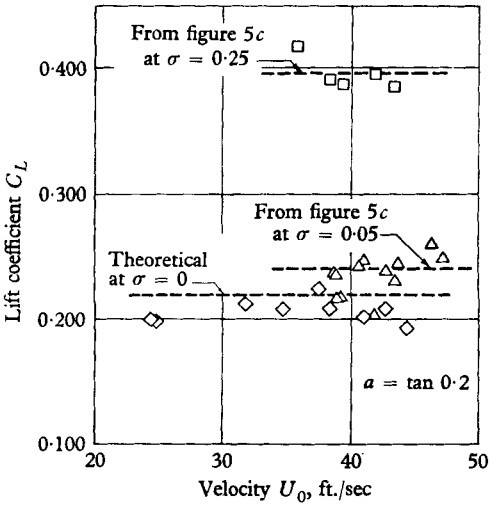

FIGURE 9. Effect of gravity on flat-plate lift coefficient.

In order to estimate the gravitational effect on force coefficients, the flat plate at an incidence of $\tan^{-1}(0{\cdot}2)$ was operated over a range of velocities at each of several cavitation numbers. The resulting lift coefficients are plotted in figure 9. Similar results were obtained for drag coefficients. It may be concluded from the figure that, within the range of velocities studied, there is no recognizable effect on force coefficients attributable to gravity. Another similar experiment was performed using the wedge of 12·5° semi-angle at zero cavitation number. These results are included in figure 4*c*. A definite decrease in drag coefficient was observed when the velocity was decreased from 27·6 to 19·4 ft./sec, but at higher velocities any change may be within the experimental error.

No experimental investigation has been made as to the effect of gravity on cavity shape. The definition for cavitation number given by (1) may be looked upon as the ratio of transverse momentum change produced by pressure difference to longitudinal momentum change. Considering that, for a given cavitation number, $p_0 - p_k$ is constant along the jet while U_0 increases because of gravity, it would be expected that a cavity in the vertical free jet would be longer than predicted by a theory obtained without considering gravity.

5. Comparison with theory and with measurements by others

In each of figures 3 to 8, one or more comparable theoretical or experimental results have been introduced.

In figure 3, for the two-dimensional cup, the theoretical drag is calculated by assuming that stagnation pressure exists uniformly over the upstream surface of the cup and that cavity pressure exists uniformly over the downstream surface. Then

$$C_D = \frac{q+p_0-p_k}{q} = 1+\sigma. \tag{8}$$

This prediction is independent of the tunnel boundary conditions (but may be influenced by the depth of the cup). The comparison between (8) and the experimental results shown in figure 3 serves to verify the drag dynamometer.

For the wedges at zero cavitation number in an infinite jet, the free-streamline theory has been worked out by Siao & Hubbard (1953). Calculations have been made from Siao & Hubbard's paper; the theoretical results for drag are indicated on the graphs of figure 4 and for shape, for the 15° wedge, by crosses on the photograph in figure 8*a* (plate 2). Agreement between measurement and theory is very satisfactory. The cavity walls seen in the downstream portion of the photograph in figure 8*a* (plate 2) have already attained their theoretical direction at infinity—6·42° with the axis of symmetry.

Cohen & Tu (1956) have developed a linearized theory for drag and cavity length of a symmetrical wedge in a free jet at non-zero cavitation numbers. The computations required to obtain drag coefficient from the paper are quite involved; but one of the authors, in a private communication, supplied the curve reproduced in figure 4*a* for the 15° semi-angle wedge. There is good agreement with the experimental data for cavitation numbers above 0·1.* Also reproduced in figure 4*a* are the results obtained on the basis of infinite-fluid theory by Plesset & Shaffer (1948) using the Riabouchinsky method and by Wu (1957) using a linearized theory. Wu's results are also plotted in figure 4*c* for comparison with the experimental results for the 12·5° semi-angle wedge. In the non-cavitating range (figure 4*b*), comparison is made with the experimental results of Lindsey (1938) obtained in a closed wind tunnel. The present results are uniformly about 13 % below those of Lindsey (which include skin friction).

Theoretical results for cavity length for the 15° semi-angle wedge are plotted with the experimental data in figure 7*a*. The effective shortening of the cavity in the free jet, as compared to a cavity in an infinite fluid, is clearly shown. The measured cavity lengths are even shorter than predicted by the linear free-jet theory, although they might have been expected to be longer because of the gravitational effect discussed in § 4. Actually, as may be seen in figures 8*c* and 8*d* (plate 2), there is considerable uncertainty in measuring cavity length; and this,

* Linear theories depend on the introduction of a perturbation potential to produce the cavity. It must be assumed that the perturbation potential will not affect the flow at infinity. However, with an infinitely long cavity, there is no way to avoid interference with the flow at infinity and the linear method must fail at zero cavitation number.

together with the breakdown of the linear theory at small cavitation numbers, may account for the discrepancies between experiment and theory.

Although the free-streamline theory for an inclined flat plate in a jet at zero cavitation number is fairly straightforward, no solution which had been carried to the point of computational usefulness could be found in the literature. Accordingly, such a solution is given in Appendix B. The calculated lift and drag coefficients are shown on the graphs in figure 5, and the resulting cavity shape for the angle of attack of $\tan^{-1}(0{\cdot}2)$ is shown on the photograph in figure 8*b* (plate 2). Agreement between experiment and theory may again be considered very satisfactory. In the downstream portion of the photograph in figure 8*b* (plate 2), the cavity walls have already become essentially straight and have attained their theoretical directions at infinity, 4·01 degrees with the axis of symmetry for the wall originating from the leading edge and 6·43 degrees for the other.

There is no available theory for the inclined plate in a jet at non-zero cavitation numbers.* For comparative purposes, the results of the free-streamline theory (non-linear) for an infinite fluid given by Wu (1956) are shown on the graphs in figure 5. The data fall below the infinite-fluid theory at small cavitation numbers, as is to be expected, and appear to approach the infinite-fluid results as the cavitation number increases. It should be observed that Wu's theoretical results agree well with experimental measurements in a closed tunnel at a chord-tunnel-width ratio of about 1/8 as reported by Parkin (1958). The experimental measurements in the closed tunnel were carried down to a cavitation number of about 0·15 at an angle of attack of 8°, down to about 0·2 at 11°, down to about 0·35 at 20°, and down to about 0·45 at 25°. In so far as lift is concerned, it appears from the present data, from Wu's theory, and from Parkin's data that wall corrections are important only at small cavitation numbers (of the order of 0·12 or less) for the narrow cavities associated with small angles of attack.

Wu's theory for the plate in an infinite fluid does not yield a precise definition of cavity length. However, lengths obtained using the definition given by Wu are shown for comparative purposes on the graphs in figures 7*c* and 7*d*. Also shown on these graphs are the cavity lengths predicted by Tulin's (1956) linear theory for the inclined plate in infinite fluid. (Lift and drag predicted by Tulin's theory were not shown in figure 5, as the curves are only a little higher than Wu's curves at zero cavitation number and approach Wu's curves closely at higher cavitation numbers.) As in the case of the wedge, there is difficulty in selecting the closing point of the cavities from the flat-plate photographs, so the experimental cavity lengths shown in the figures are subject to some error. The results look reasonable, however, when compared with the infinite-fluid theory.

Three theoretical drag coefficients computed for the circular cylinder in infinite fluid, presented by Birkhoff & Zarantonello (1957, p. 148) are shown for comparison with the experimental data in figure 6*a*. The agreement with free-jet data is quite good at all three points. At higher cavitation numbers, shown in figure 6*b*, comparison is made with Martyrer's experimental data (1932) obtained in a closed

* There is a fundamental obstacle to the development of a suitable linear theory for a lifting surface in a jet because of the absence of symmetry in both the cavity and the jet walls.

tunnel. Again agreement between the free-jet and closed-tunnel results is reasonably good. For the non-cavitating flow past the circular cylinder (figure 6*c*), the accepted value for the drag coefficient at Reynolds numbers from 2 to 4×10^4 is about 1·2, as given in Prandtl & Tietjens (1934, figure 50, p. 96). Small discrepancies between free-jet and closed-tunnel results may be accounted for by variations in the point of separation on the cylinder.

6. Conclusion

Good agreement has been obtained between measurements in the free-jet tunnel and theoretical prediction for a free jet, where theoretical predictions were available. At the operating speeds of the tunnel, gravity has no appreciable effect on the measured force coefficients. The tunnel and measuring equipment are, therefore, believed to be operating satisfactorily.

Comparison between the present results and theoretical results for an infinite fluid, and with measurements by others in closed tunnels, indicates that wall corrections for converting measured results in the free jet to infinite-fluid conditions are negligibly small for all but the smallest cavitation numbers. At zero cavitation number, force coefficients and cavity lengths measured in the free jet can be expected to be less than those in infinite fluid. The exact relation depends on the shape of the body and its position in the jet. For the flat plate at several angles of attack, the difference between the measurements in the jet and the theoretical predictions for infinite fluid all but disappeared for cavitation numbers greater than about 0·12.

The work described herein was undertaken at the St Anthony Falls Hydraulic Laboratory with support of the Office of Naval Research, United States Department of the Navy, under contract Nonr 710(24) with the University of Minnesota. Robert L. Gordier has been responsible for operating the tunnel and obtaining the experimental data. John F. Ripken has been of material assistance in perfecting the experimental equipment and in offering advice on other phases of the work.

Appendix A

Drag corrections

Two subtractive corrections were made to the measured drag coefficients. The first of these, the end-disk drag, was calculated by assuming a turbulent (dictated by the Reynolds number) flat-plate boundary layer from the leading edge of each side plate. The local shear stress was then integrated over the area of each disk less an average area occupied by the body plus cavity or wake. No allowance was made for pressure drag on the disks even though there was a little leakage around their edges. The final expression for the correction to the drag coefficient for the two end disks was

$$\Delta C_D = -\frac{0{\cdot}0605}{\mathrm{Re}^{\frac{1}{5}}}\left(\frac{R}{c}\right)^{\frac{4}{5}}, \tag{A 1}$$

where R is the radius of the end disk—i.e. 1·27 in.

The calculations were partially checked by measurements in the tunnel. A flat plate of 2 in. chord and at an incidence of $\tan^{-1}(0{\cdot}2)$ was mounted rigidly as a cantilever beam from the lift side plate with the lift dynamometer removed. A dummy end disk was mounted in the drag dynamometer; about 0·004 in. separated the disk from the flat plate. Drag measurements obtained with this arrangement were about 25 % lower than given by the above formula. It was later realized, however, that pressure differences over the face of the disk caused the disk to twist out of the plane of the wall, twisting the dynamometer and producing false readings which could be expected to be low.

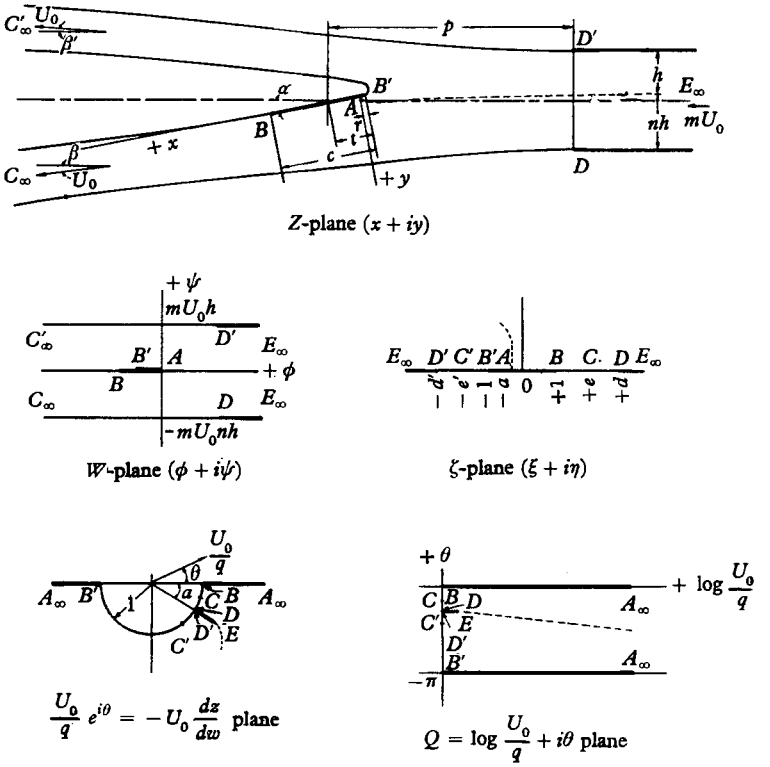

FIGURE 10. Conformal mapping planes.

The second correction was for skin-friction drag on the test bodies. The wedges, being of 1 in. chord, possessed laminar boundary layers. Drag was calculated using the wedge-flow solution as outlined in Schlichting (1955, p. 128). For application of this solution, the velocity was taken in the form

$$U(x) = U_k x^m = U_0(1+\sigma)^{\frac{1}{2}} x^m, \tag{A 2}$$

where x is the distance along the wedge from the front stagnation point, in inches ($0 \leqslant x \leqslant 1$), $U(x)$ is the velocity at any x, U_k is the constant velocity at the edge of the cavity given by $(U_k/U_0)^2 = 1+\sigma$, and $m = \gamma/(\pi-\gamma)$ where γ is the wedge semi-angle. Integration of the wall shear stress over both surfaces resulted in the expression

$$\Delta C_D = -C\frac{(1+\sigma)^{\frac{3}{4}}}{\mathrm{Re}^{\frac{1}{2}}}, \tag{A 3}$$

where the constant C has the value 1·91 for the 12·5° semi-angle wedge and 2·20 for the 15° semi-angle wedge. It is noted in passing that if each wedge surface had been considered a flat plate at zero pressure gradient in a stream of velocity U_0, the constants would have been 1·77 and 1·94, respectively, at zero cavitation number.

In view of the wedge solution and the comparison with the flat plate at zero pressure gradient just discussed, skin friction on the inclined flat plates (one side only) was based on the skin friction of the flat plate at zero pressure gradient. For laminar boundary layers, equation (A 3) was used, C having the value 1·328. For turbulent boundary layers, which occurred on the 2 in. chord plate, $0{\cdot}074/\mathrm{Re}^{\frac{1}{5}}$ was substituted for $C/\mathrm{Re}^{\frac{1}{2}}$ in equation (A 3).

Only the end-disk skin-friction correction was applied to the cup and circular cylinder data.

Appendix B

Free-streamline solution for an inclined flat plate in an infinite jet

The upper diagram in figure 10 represents the flow from a jet from a nozzle about an inclined flat plate. The corresponding complex-potential plane and other mapping planes are shown in the remaining diagrams. The origin in the physical plane is taken at the stagnation point A. The angle of attack is α and the velocity on the free streamline is U_0. The transformations are

$$\left.\begin{aligned} W &= \frac{mU_0h}{\pi}\left[n\log\frac{\zeta-e}{e+a}+\log\frac{\zeta+e'}{e'-a}-i\pi n\right], \\ n &= \frac{e+a}{e'-a}, \end{aligned}\right\} \tag{B 1}$$

$$\frac{dQ}{d\zeta} = \frac{K}{(\zeta+a)\,[(\zeta^2-1)\,(\zeta-d)\,(\zeta+d')]^{\frac{1}{2}}}. \tag{B 2}$$

Equation (B 2) is readily integrated when points D and D' are at infinity in the ζ plane (p goes to infinity in the physical plane while $h+nh$ remains constant). This corresponds to the case of the infinite jet with $m = 1$. Then

$$Q = -\cosh^{-1}\left(\frac{1+a\zeta}{\zeta+a}\right) = -\log\left\{\frac{1+a\zeta}{\zeta+a}-\left[\left(\frac{1+a\zeta}{\zeta+a}\right)^2-1\right]^{\frac{1}{2}}\right\}, \tag{B 3}$$

$$-U_0\frac{dz}{dw} = \frac{1+a\zeta+i[(1-a^2)\,(\zeta^2-1)]^{\frac{1}{2}}}{\zeta+a}, \tag{B 4}$$

$$a = \cos\alpha, \tag{B 5}$$

$$\left.\begin{aligned} \beta &= -\alpha+\tan^{-1}\left[\frac{(e^2-1)^{\frac{1}{2}}\sin\alpha}{1+e\cos\alpha}\right], \\ \beta' &= -\alpha+\tan^{-1}\left[\frac{(e'^2-1)^{\frac{1}{2}}\sin\alpha}{e'\cos\alpha-1}\right], \end{aligned}\right\} \tag{B 6}$$

$$\frac{dz}{d\zeta} = -\frac{h(n+1)}{\pi}\,\frac{1+a\zeta+(1-a^2)^{\frac{1}{2}}\,(1-\zeta^2)^{\frac{1}{2}}}{(\zeta+e')\,(\zeta-e)}; \tag{B 7}$$

and, for $\zeta^2 \leqslant 1$,

$$\frac{z}{h(n+1)} = \frac{1}{\pi(e'+e)}\left[(ae+1)\log\frac{a+e}{e-\zeta} - (ae'-1)\log\frac{e'+\zeta}{e'-a}\right] + \frac{\sin\alpha}{\pi}\left\{\pi - \alpha - \cos^{-1}\zeta \right.$$
$$+ 2\frac{(e'^2-1)^{\frac{1}{2}}}{e'+e}\tan^{-1}\frac{[(1-a)(1-\zeta)]^{\frac{1}{2}} - [(1+a)(1+\zeta)]^{\frac{1}{2}}}{[(1-a)(1+\zeta)(e'+1)/(e'-1)]^{\frac{1}{2}} + [(1+a)(1-\zeta)(e'-1)/(e'+1)]^{\frac{1}{2}}}$$
$$\left. + 2\frac{(e^2-1)^{\frac{1}{2}}}{e'+e}\tan^{-1}\frac{[(1-a)(1-\zeta)]^{\frac{1}{2}} - [(1+a)(1+\zeta)]^{\frac{1}{2}}}{[(1-a)(1+\zeta)(e-1)/(e+1)]^{\frac{1}{2}} + [(1+a)(1-\zeta)(e+1)/(e-1)]^{\frac{1}{2}}}\right\}. \tag{B 8}$$

The constant was evaluated so that $z = 0$ when $\zeta = -a$. Noting that the chord length is given by $c = z_{B'} - z_B$, the chord-length to jet-width ratio is found to be

$$\frac{c}{h(n+1)} = \left[1 - \frac{(e'^2-1)^{\frac{1}{2}} + (e^2-1)^{\frac{1}{2}}}{e'+e}\right]\sin\alpha - \frac{ae'-1}{\pi(e'+e)}\log\frac{e'+1}{e'-1} + \frac{ae+1}{\pi(e'+e)}\log\frac{e+1}{e-1}. \tag{B 9}$$

For $\zeta^2 \geqslant 1$, the integral of (B 7) may be written

$$\frac{z}{h(n+1)} = \frac{1}{\pi(e'+e)}\left[(ae'-1)\log\frac{e'-a}{e'+\zeta} - (ae+1)\log\frac{e-\zeta}{a+e}\right] - \frac{\alpha}{\pi}\sin\alpha$$
$$+ \frac{2\sin\alpha}{\pi(e'+e)}\left[(e'^2-1)^{\frac{1}{2}}\tan^{-1}\left(\frac{e'+1}{e'-1}\frac{1-a}{1+a}\right)^{\frac{1}{2}} + (e^2-1)^{\frac{1}{2}}\tan^{-1}\left(\frac{e-1}{e+1}\frac{1-a}{1+a}\right)^{\frac{1}{2}}\right]$$
$$+ i\frac{\sin\alpha}{\pi}\left\{\cosh^{-1}(-\zeta) - \frac{2}{e'+e}\left[(e'^2-1)^{\frac{1}{2}}\tanh^{-1}\left(\frac{e'+1}{e'-1}\frac{\zeta+1}{\zeta-1}\right)^{\frac{1}{2}}\right.\right.$$
$$\left.\left. + (e^2-1)^{\frac{1}{2}}\tanh^{-1}\left(\frac{e-1}{e+1}\frac{\zeta+1}{\zeta-1}\right)^{\frac{1}{2}}\right]\right\}. \tag{B 10}$$

The positions of the upper and lower jet walls at E with respect to A in the physical plane are given by

$$\tfrac{1}{2}h(n+1) - (t-r)\sin\alpha = -x_{E(-\infty)}\sin\alpha - y_{E(-\infty)}\cos\alpha, \tag{B 11}$$

$$\tfrac{1}{2}h(n+1) + (t-r)\sin\alpha = x_{E(+\infty)}\sin\alpha + y_{E(+\infty)}\cos\alpha. \tag{B 12}$$

Subtracting (B 11) from (B 12), we find

$$\frac{t}{h(n+1)} = \tfrac{1}{2}\sin\alpha + \frac{\cos\alpha}{\pi}\log 2 + \frac{1}{e'+e}\left\{\cot\alpha - (e'-e)\frac{\sin\alpha}{2}\right.$$
$$- (e'^2-1)^{\frac{1}{2}}\sin\alpha - \frac{1}{\pi}\log\frac{e'-1}{e+1} - \frac{\cos\alpha}{(e'+e)\pi}\left[2(e'^2-1)^{\frac{1}{2}}\tanh^{-1}\left(\frac{e'-1}{e'+1}\right)^{\frac{1}{2}}\right.$$
$$\left.\left. - e'\log(e'-1) + 2(e^2-1)^{\frac{1}{2}}\tanh^{-1}\left(\frac{e-1}{e+1}\right)^{\frac{1}{2}} - e\log(e+1)\right]\right\}. \tag{B 13}$$

Equations (B 9) and (B 13) are a pair of simultaneous equations for e and e', given c, t, $h(n+1)$, and α. Once e and e' are determined, lift and drag may be obtained from the momentum equation using (B 6) or by integrating the pressure

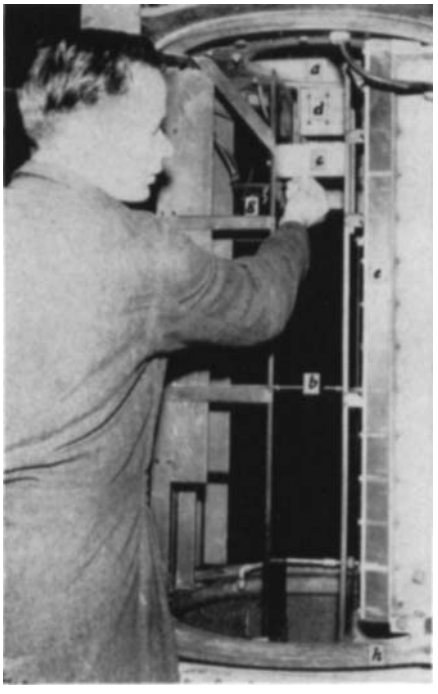

Elevation

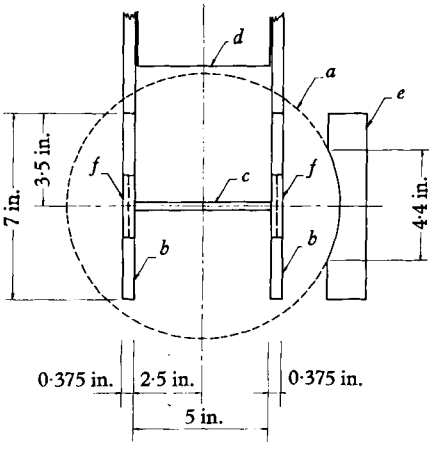

Plan

FIGURE 2 (plate 1). Views of two-dimensional test section. *a*, 10 in. diameter free jet nozzle; *b*, two-dimensional side plates; *c*, test body and integral end disks; *d*, side plate support structure; *e*, viewing window (Plexiglass), *f*, dynamometers; *g*, piezometer tubes for measuring cavity pressure; *h*, housing that rises to seal test section.

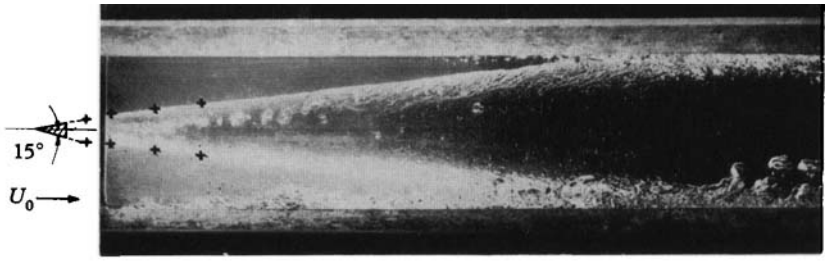

+Theoretical points
(*a*) Symmetrical wedge, $\sigma = 0$

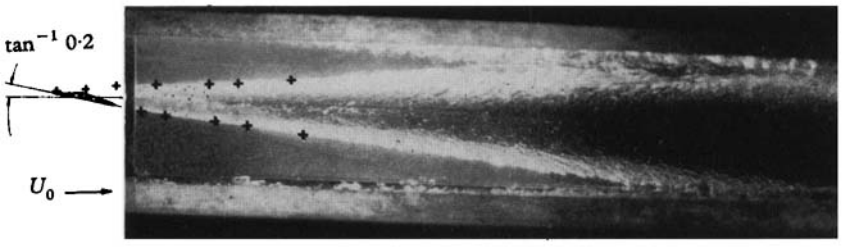

+Theoretical points
(*b*) Flat plate, $\sigma = 0$

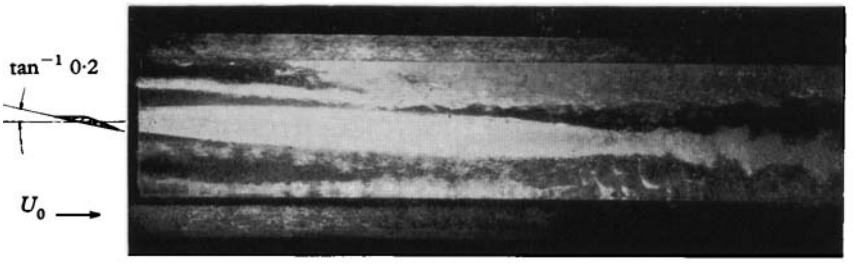

(*c*) Flat plate, $\sigma = 0{\cdot}063$

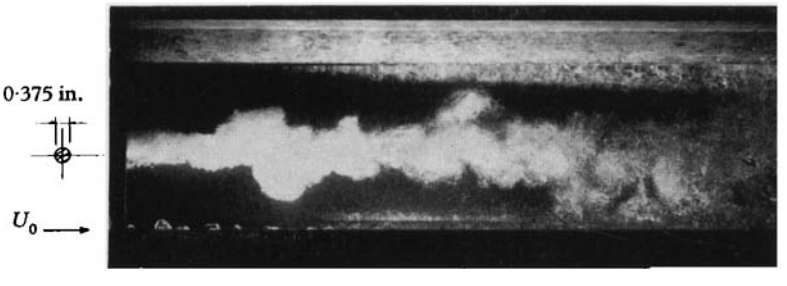

(*d*) Circular cylinder, $\sigma = 0{\cdot}301$

FIGURE 8 (plate 2). Typical cavities.

over the plate. Performing either of these operations, and reducing the results to coefficient form, we obtain

$$C_L = \frac{\pi \sin 2\alpha}{\pi \sin \alpha + \dfrac{(ae'-1)\log[(e'+1)/(e'-1)] - (ae+1)\log[(e+1)/(e'-1)]}{(e^2-1)^{\frac{1}{2}} + (e'^2-1)^{\frac{1}{2}} - e' - e}}, \tag{B 14}$$

and

$$C_D = C_L \tan \alpha. \tag{B 15}$$

When the fluid is infinite, h, e and $e' \to \infty$, and

$$C_{L\infty} = \frac{\pi \sin 2\alpha}{\pi \sin \alpha + 4}. \tag{B 16}$$

Hence

$$\frac{C_L}{C_{L\infty}} = \frac{C_D}{C_{D\infty}} = \frac{h(n+1)}{c}(4/\pi + \sin\alpha)\left[1 - \frac{(e'^2-1)^{\frac{1}{2}} + (e^2-1)^{\frac{1}{2}}}{e'+e}\right]. \tag{B 17}$$

Equation (B 17) is plotted in figure 11 for several angles of attack for the case $t/c = \frac{1}{3}$. Small changes in t/c have negligible effect on the force coefficients.

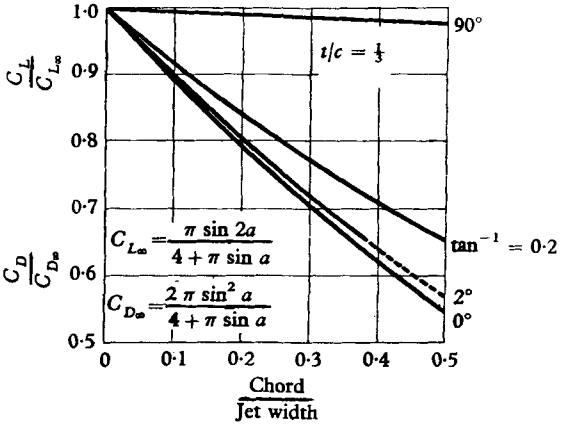

FIGURE 11. Force coefficients for flat plates in free jet at zero cavitation number.

REFERENCES

BIRKHOFF, G., PLESSET, M. S. & SIMMONS, N. 1950 Wall effects in cavity flow. Part I. *Quart. Appl. Math.* **8**, 151.

BIRKHOFF, G., PLESSET, M. S. & SIMMONS, N. 1952 Wall effects in cavity flow. Part II. *Quart. Appl. Math.* **9**, 413.

BIRKHOFF, G. & ZARANTONELLO, E. H. 1957 *Jets, Wakes and Cavities.* New York: Academic Press.

CHRISTOPHERSON, C. D. 1953 Description of a ten-inch free-jet water tunnel. *St Anthony Falls Hydraulic Laboratory, University of Minnesota, Project Rep.* no. 35. (Available on interlibrary loan from the University of Minnesota Library, Minneapolis 14, Minnesota.)

COHEN, H. & TU, Y. 1956 A comparison of wall effects on supercavitating flows past symmetric bodies in solid wall channels and jets. *Proc. 9th Int. Congr. Appl. Mech., Brussels*, p. 359.

LINDSEY, W. F. 1938 Drag of cylinders of simple shapes. *Nat. Adv. Comm. Aero., Wash., Rep.* no. 619.

MARTYRER, E. 1932 Kraftsmessungen an Widerstandskörpern und Flügelprofilen in Wasserstrom beim Kavitation, Article in *Hydromechanische Probleme des Schiffsentriebs* (Ed. Kempf & Foerster). Hamburg: Schiffbau–Versuchsanstalt.

PARKIN, B. R. 1958 Experiments on circular arc and flat plate hydrofoils in noncavitating and full cavity flows. *J. Ship. Res.* **1**, 34.

PLESSET, M. S. & SHAFFER, P. A., JR. 1948 Cavity drag in two and three dimensions. *J. Appl. Phys.* **19**, 934.

PRANDTL, L. & TIETJENS, O. G. 1934 *Applied Hydro and Aeromechanics.* New York: McGraw-Hill.

SCHLICHTING, H. 1955 *Boundary Layer Theory.* New York: McGraw-Hill.

SIAO, T. T. & HUBBARD, P. G. 1953 Deflection of jets, Part I. Symmetrically placed V-shaped obstacle. *Free Streamline Analyses of Transition Flow and Jet Deflection, State University of Iowa, Bulletin* no. 35, p. 33.

TULIN, M. P. 1956 Supercavitating flow past foils and struts. *Proc. Symposium on Cavitation in Hydrodynamics, National Physical Laboratory, Teddington, England.*

WU, T. Y. 1956 A free streamline theory for two-dimensional fully cavitated hydrofoils. *J. Math. Phys.* **25**, 236.

WU, T. Y. 1957 A simple method for calculating the drag in the linear theory of cavity flows. *California Institute of Technology, Rep.* no. 85.